Double photoionization of molecular hydrogen: A theoretical study including the nuclear dissociation

H. Le Rouzo
Laboratoire de Photophysique Moléculaire du CNRS, Batiment 213, Université Paris-Sud 91405 Orsay Cédex, France and Institut Universitaire de Technologie de Troyes, 9, Rue de Québec, Boîte Postale 396, 10026 Troyes Cédex, France
(Received 26 June 1987)

The double photoionization of molecular hydrogen is theoretically investigated in the 40–100-eV photon energy range. The calculation is *ab initio* and rests first on the Born-Oppenhiemer separation. The exact nuclear wave functions have been used for both (bound) initial and (dissociative) final two-proton states and the Franck-Condon approximation is not invoked. The electronic part of the initial ground state of H_2 is highly correlated while the final one is simply a symmetrized product of uncorrelated Coulomb wave functions. Within this framework, the total cross sections obtained in the dipole-velocity formulation agree well with very recent experimental results. In addition, the method is able to provide the kinetic-energy distributions of the fragments (electrons and protons) as functions of the photon energy. The energy distributions of the ejected protons, produced by 60–100-eV impacting photons, are similar in shape to those resulting from electron or proton impact on H_2. In contrast, it is found that the most probable two-proton kinetic energy is significantly lowered in the threshold region. On the other hand, the differential electron spectrum gives some insights into the sharing of energy between the *s*, *p*, and *d* ejected electrons. Within the δ approximation, which is shown to be very accurate over the whole photon energy range, the threshold law for the double photoionization of diatomic molecules is derived. It is found that the cross sections can be represented, up to 10 eV above threshold, as the convolution of the density probability in the initial vibrational ground state with a series of linear thresholds, similar to those derived in the Wannier-Rau-Peterkop theory for atoms.

I. INTRODUCTION

Interest in the double photoionization (DPI) of neutral molecules has been recently renewed by the conjoined utilization of tunable synchrotron radiation and the photoion-photoion-coincidence (PIPICO) method. For numerous small molecules,[1] this new technique has provided detailed data on the doubly charged cations that dissociate into fragments.

Corresponding to this experimental activity, several *ab initio* calculations of potential-energy curves of doubly charged cations have been performed with the aid of methods that have long been used in the study of molecular structure. Going from the lowest to the highest sophistication, the low-lying states of the cations can be investigated with Koopman's approximation, self-consistent-field (SCF), configuration-interaction, and multi-configuration-SCF approaches. Due to the high density of accessible states (note, e.g., that triplet states are often populated by DPI) such investigations are not easy. However, they have been successful in identifying threshold values of many accessible dissociative states of the doubly charged cations.[2]

Unfortunately, such calculations do not yield the properties related to the electronic transition moment, like cross sections or kinetic and angular distributions of fragments. This lack of information was the major motivation for our previous study of the DPI of molecular hydrogen[3] (hereafter, this work will be referred to as paper I), which to our knowledge is the first study of a *molecular* DPI reaction. In this work, we performed a DPI calculation of the kind adopted by Byron and Joachain[4] in their pioneering work on helium. Following these authors, we used a highly correlated electronic wave function for the initial ground state of H_2, and represented the final states simply by symmetrized products of uncorrelated Coulomb wave functions. This model has provided rather good information concerning the ejected electrons. However, due to the fact that the calculation was performed for the *fixed* ground-state equilibrium geometry, no quantitative information related to protons could be extracted. Hence, in order to set up a more complete *molecular* "wave-function approach" of the DPI, it is worthwhile to take the nuclear motion into account. In spite of the dissociative nature of the final cation H_2^{2+}, we shall address this problem by use of the Born-Oppenheimer approximation. This yields a slightly more involved model than in paper I, since the final states now comprise four particles (two protons and two electrons) instead of only two electrons. Moreover, some conceptual modifications of the theory reported in paper I are necessary since, e.g., the two sets of electrons and protons no longer have separate definite energies.

The organization of the present paper is as follows. Sections II and III are devoted to the description of the wave functions describing the initial ground state of H_2

and the final states accessible via the DPI process. In Sec. IV, the cross-section formulas are derived in a model where rotation is neglected while nuclear motion is properly averaged. Computational details are given in Sec. V. Finally, results are presented and discussed in Sec. VI.

II. GROUND-STATE WAVE FUNCTION

In the molecular frame, the Born-Oppenheimer approximation allows the vibronic wave function of the $X\,^1\Sigma_g^+$ ground state of the hydrogen molecule to be factored as

$$\Psi_i(X\,^1\Sigma_g^+,E_i,v \mid \mathbf{r}_1,\mathbf{r}_2,R) = \Phi_i(X\,^1\Sigma_g^+,R \mid \mathbf{r}_1,\mathbf{r}_2)R^{-1}P_i(v \mid R) , \quad (1)$$

where R is the nuclear separation and $\mathbf{r}_k$ is the position vector of the kth electron.[5] The index i will be used to denote quantities referring to the initial state. The electronic and vibrational parts of the wave function, Φ_i and P_i, respectively, are both normalized to unity. It should be noted that the spin part of a two-electron wave function can be factored out, so that spin will be ignored in the rest of the paper. As usual, the fixed-nuclei electronic Schrödinger equation is solved first to yield the eigenfunction Φ_i and the (negative) associated eigenvalue E_i^e, for various geometries. The purely electronic energy $E_i^e(R)$ plus the nuclear potential energy $1/R$ yield the Born-Oppenheimer potential-energy curve that governs the motion of nuclei. More precisely, the vibrational eigenvalues and eigenfunctions of the vth level are obtained from

$$\left[\frac{d^2}{dR^2}+2\mu\left[E_i^n(v)-E_i^e(R)-\frac{1}{R}\right]\right]P_i(v \mid R)=0 , \quad (2)$$

where μ is the reduced nuclear mass. In this paper, except when explictly notified, atomic units are used.[6] Hence, μ is expressed in units of the electron rest mass and we adopt $\mu=918.05$. Finally, the energy of the initial vibronic state is

$$E_i=E_i^e(R_e)+\frac{1}{R_e}+E_i^n(v=0) , \quad (3)$$

where $R_e=1.4$ bohr is the equilibrium nuclear separation.

A key result of the work of Byron and Joachain[4] was the recognition of the importance of ground-state electronic correlation in the DPI of helium. They expanded the $\Phi_i(1\,^1S_0)$ ground-state wave function of helium in terms of three relative partial waves and obtained an energy of -2.9020 hartree, indicating that their 45-parameter Ψ_i accounts for 95.9% of the correlation energy.[7] With the very accurate six-parameter Hylleraas wave function (yielding an energy of -2.9033 hartree and thus including 99.0% of the correlation energy), Brown[8] obtained essentially the same ratio of double- to single-ionization cross sections as did Byron and Joachain. This indicates that, although partly optimized, the ground-state wave function of Byron and Joachain was sufficiently correlated. Since the helium atom and the hydrogen molecule are very similar two-electron systems as far as electronic correlation is concerned,[9] we are led to adopt a ground-state wave function for H_2 of nearly the same accuracy, i.e., accounting for, say, more than 90% of the correlation energy. Such high accuracies have long been achieved for two-electron systems either by the explicit inclusion of the interelectronic distance r_{12} in the wave functions, or, alternatively, by use of superposition of configurations constructed with single-particle orbitals. In this work, as in paper I, we have adopted the latter approach by choosing configuration interaction wave functions of the form optimized by Hagström and Shull.[10] As will be described in more detail in Sec. V, this ensures that more than 95% of the ground-state correlation energy is accounted for in the considered geometries.

III. FINAL-STATE WAVE FUNCTIONS

As mentioned in the Introduction, the DPI of H_2 is dissociative and so leads to final states that are unbounded with respect to *both* electronic and nuclear degrees of freedom. Nevertheless, we assume that the Born-Oppenheimer approximation still applies, so that a final-state wave function should read (in the body frame)

$$\Psi_f(S,l,E_f^e,E_f^n \mid \mathbf{r}_1,\mathbf{r}_2,R) = \Phi_f(S,l,E_f^e,R \mid \mathbf{r}_1,\mathbf{r}_2)R^{-1}P_f(E_f^n \mid R) , \quad (4)$$

where S is the set of symmetry quantum numbers and l is an index (to be defined below) used to distinguish the degenerate final states having total energy E_f. Note that the index f will be used to denote quantities referring to final states. The total energy splits into electronic and nuclear positive contributions as

$$E_f=E_f^e+E_f^n , \quad (5)$$

and it should be stressed that any partitioning of E_f is *a priori* allowed. The electric-dipole selection rules, for single-photon absorption, state that only final states with $S=\,^1\Sigma_u^+$ or $^1\Pi_u$ symmetries are accessible from the $X\,^1\Sigma_g^+$ ground state of the molecule.

We consider first the determination of the nuclear wave function. The actual potential energy is that of H_2^{2+}, i.e., it corresponds to the Coulombic repulsion of two protons. Consequently, one has

$$\left[\frac{d^2}{dR^2}+2\mu\left[E_f^n-\frac{1}{R}\right]\right]P_f(E_f^n \mid R)=0 . \quad (6)$$

Given any positive energy E_f^n it is possible to solve Eq. (6) for $P_f(E_f^n \mid R)$ via standard numerical procedures. However, it is readily recognized that Eq. (6) defines the so-called spherical Coulomb functions of order 0, which can be computed with very efficient existing algorithms. In the notation of Abramowitz and Stegun[11] the regular solution reads

$$P_f(E_f^n \mid R)=F_0(\eta_n \mid k_nR) \quad (7)$$

with

$$k_n=(2\mu E_f^n)^{1/2}, \quad \eta_n=\mu/k_n . \quad (8)$$

Coulomb functions oscillate with amplitudes approaching unity in the limit of infinite R. They are conveniently normalized in the energy scale[12] by use of a Dirac distribution

$$\int_0^\infty P_f(E \mid R)P_f(E' \mid R)dR=\delta(E-E') . \tag{9}$$

Applying this condition, the normalized nuclear wave functions are easily expressed as

$$R^{-1}P_f(E_f^n \mid R)=\left[\frac{2\mu}{k_n\pi}\right]^{1/2}\frac{F_0(\eta_n \mid k_nR)}{R} . \tag{10}$$

In the theory of the dissociation of diatomic molecules by electron, proton, or photon impact, it is a common practice to substitute a δ function at the classical turning point for the nuclear continuum wave functions.[13] This "δ" or "reflection" approximation is especially useful when the position and shape of the upper potential are not known. Here, although we are able to deal with the *exact* nuclear functions describing the actual dissociative two-proton final state, it is interesting to consider this approximation along with the exact treatment. Let $R_f^n=1/E_f^n$ be the classical turning point for the nuclear state of energy E_f^n. It can be proved (see the Appendix) that the approximate wave function

$$R^{-1}P_f(E_f^n \mid R)\simeq\frac{1}{E_f^n}\frac{\delta(R-R_f^n)}{R} \tag{11}$$

is properly normalized as required by Eq. (9). In spite of its simplicity, it will be seen that the function represented by Eq. (11) is a rather good approximation of the exact one [Eq. (10)].

We now arrive at the major difficulty encountered within the wave-function approach of atomic or molecular species, namely, the determination of the wave function Φ_f representing the two ejected electrons. For the helium problem, Byron and Joachain[4] have chosen a model with independent electrons. Using single-electron spatial orbitals $\phi(\varepsilon,l,m \mid \mathbf{r})$ with the asymptotic kinetic-energy ε and angular quantum numbers (l,m), they have constructed configurations of the type $\varepsilon l\,\varepsilon'(l+1)$ with asymptotic electronic energy

$$E_f^e=\varepsilon+\varepsilon' . \tag{12}$$

The precise form of the properly symmetrized final-state wave functions they used is

$$\Phi_f({}^1P_M,l,\varepsilon,\varepsilon' \mid \mathbf{r}_1,\mathbf{r}_2)=\frac{1}{\sqrt{2}}\sum_{m=-l}^{+l}(l,m,l+1,M-m \mid 1,M)[\phi(\varepsilon,l,m \mid \mathbf{r}_1)\phi(\varepsilon',l+1,M-m \mid \mathbf{r}_2)+1\leftrightarrow 2] , \tag{13}$$

where $(l_1,m_1,l_2,m_2 \mid 1,M)$ denotes the Clebsch-Gordan coefficients providing the desired final state ${}^1P_M$. In Eq. (13), the one-electron spatial orbitals are given by

$$\phi(\varepsilon,l,m \mid \mathbf{r})=\left[\frac{2}{k_e\pi}\right]^{1/2}\frac{F_l(\eta_e \mid k_er)}{r}\mathcal{Y}_{lm}(\hat{r}) , \tag{14}$$

where $F_l(\eta_e \mid k_er)$ is the regular spherical Coulomb function of order l with

$$k_e=\sqrt{2\varepsilon} \text{ and } \eta_e=-Z/k_e . \tag{15}$$

Byron and Joachain[4] have taken the effective charge $Z=2$. This choice corresponds to the situation where each electron does not screen the nuclear charge seen by the other one. One can expect that this is physically reasonable for two ejected electrons which are close to the nuclei for only a short time. It should be noted that the ϕ orbitals defined in Eq. (14) are again normalized in the energy scale, i.e.,

$$\langle\phi(\varepsilon,l,m) \mid \phi(\varepsilon',l',m')\rangle=\delta_{(\varepsilon-\varepsilon')}\delta_{l,l'}\delta_{m,m'} . \tag{16}$$

In the present work, as in paper I, we use for H_2 the wave function devised for the helium atom. This approximation was expected to be reasonable since it was known that Coulomb functions provide rather accurate results for the simple photoionization of molecular hydrogen.[14] The ${}^1P_0$ and ${}^1P_{\pm1}$ atomic states represented in Eq. (13) are hence the ansatz for the corresponding ${}^1\Sigma_u^+$ and ${}^1\Pi_u^{\pm1}$ final molecular states. Finally, to summarize the above definitions, a final wave function with total energy $E_f=\varepsilon+\varepsilon'+E_f^n$ will be denoted as

$$\Psi_f(S,l,E_f^e,E_f^n \mid \mathbf{r}_1,\mathbf{r}_2,R)=\Psi_f(\mathcal{F},E_f^n \mid \mathbf{r}_1,\mathbf{r}_2,R) , \tag{17}$$

where $\mathcal{F}$ is the shorthand notation

$$\mathcal{F}\equiv\{S={}^1\Sigma_u^+,{}^1\Pi_u^{\pm1},l,\varepsilon,\varepsilon'\} \tag{18}$$

defining the pair of ejected electrons.

IV. FORMULAS FOR CROSS SECTIONS

Cross sections for molecular processes involving absorption into a continuum are conveniently expressed with the aid of differential oscillator strengths. The value of this concept mainly rests on the fact that discrete and differential oscillator strengths join smoothly at the ionization threshold.[15]

In the present problem, the accessible final states involve three such continua: two electronic ones and a single nuclear one, associated to the relative motion of protons. The relevant differential cross section is then triply differential in the energies ε, ε', and E_f^n. Under the electric-dipole approximation, the differential cross section for ejection of two electrons $\varepsilon l,\varepsilon'(l+1)$ with energies in the ranges $d\varepsilon$, $d\varepsilon'$, and for the simultaneous production of two protons with relative kinetic-energy E_f^n in the range dE_f^n, is

$$d^3\sigma^{2+}(\mathcal{F},E_f^n \mid E_\gamma) = \frac{4\pi^2\alpha a_0^2}{3}\left[\frac{\partial^3 f(\mathcal{F},E_f^n \mid E_\gamma)}{\partial\varepsilon\,\partial\varepsilon'\partial E_f^n}\right] d\varepsilon\, d\varepsilon' dE_f^n \ , \tag{19}$$

where E_γ is the photon energy. The differential oscillator strength in large parentheses in Eq. (19) is alternatively expressed in the so-called "length" (L) and "velocity" (V) forms as

$$\frac{\partial^3 f(\mathcal{F},E_f^n \mid E_\gamma)}{\partial\varepsilon\,\partial\varepsilon'\partial E_f^n} = E_\gamma \mid \underline{M}_L(\mathcal{F},E_f^n) \mid^2 = E_\gamma^{-1} \mid \underline{M}_V(\mathcal{F},E_f^n) \mid^2 , \tag{20}$$

where $\underline{M}_{L,V}$ are the dipole-matrix elements defined as

$$\underline{M}_L(\mathcal{F},E_f^n) = \langle \Psi_f(\mathcal{F},E_f^n \mid \mathbf{r}_1,\mathbf{r}_2,R) \mid \mathbf{r}_1+\mathbf{r}_2 \mid \Psi_i(X\,^1\Sigma_g^+,E_i,v=0) \mid \mathbf{r}_1,\mathbf{r}_2,R) \rangle \ , \tag{21a}$$

$$\underline{M}_V(\mathcal{F},E_f^n) = \langle \Psi_f(\mathcal{F},E_f^n \mid \mathbf{r}_1,\mathbf{r}_2,R) \mid \nabla_1+\nabla_2 \mid \Psi_i(X\,^1\Sigma_g^+,E_i,v=0) \mid \mathbf{r}_1,\mathbf{r}_2,R) \rangle \ , \tag{21b}$$

since only transitions from the $v=0$ initial ground state are considered in this work. Inserting the actual expressions for initial [Eq. (1)] and final [Eq. (4)] wave functions in Eqs. (21) leads to the usual integral over the nuclear separation

$$\underline{M}_{L,V}(\mathcal{F},E_f^n) = \int_0^\infty P_f(E_f^n \mid R)\,\underline{M}_{L,V}^e(\mathcal{F} \mid R)\,P_i(v=0 \mid R)\,dR \ . \tag{22}$$

In Eq. (22), $\underline{M}_{L,V}^e$ are the electronic dipole-matrix elements to be computed within fixed nuclear geometries

$$\underline{M}_L^e(\mathcal{F} \mid R) = \langle \Phi_f(\mathcal{F},R \mid \mathbf{r}_1,\mathbf{r}_2) \mid \mathbf{r}_1+\mathbf{r}_2 \mid \Phi_i(X\,^1\Sigma_g^+,R \mid \mathbf{r}_1,\mathbf{r}_2) \rangle \ , \tag{23a}$$

$$\underline{M}_V^e(\mathcal{F} \mid R) = \langle \Phi_f(\mathcal{F},R \mid \mathbf{r}_1,\mathbf{r}_2) \mid \nabla_1+\nabla_2 \mid \Phi_i(X\,^1\Sigma_g^+,R \mid \mathbf{r}_1,\mathbf{r}_2) \rangle \ . \tag{23b}$$

In the case where one uses the δ approximation for the nuclear wave function [Eq. (11)], the integration over R in Eq. (22) is readily performed and yields

$$\underline{M}_{L,V}(\mathcal{F},E_f^n) \simeq \frac{1}{E_f^n}\underline{M}_{L,V}^e(\mathcal{F} \mid R_f^n)P_i(v=0 \mid R_f^n) \ , \tag{24}$$

so that the electronic dipole-matrix elements $\underline{M}_{L,V}^e$ are simply modulated by the value of the initial vibrational wave function at the classical turning point. This is the mathematical foundation of the δ or reflection approximation.[13] It should be noted that this approximation is often used together with the additional assumption that electronic moments do not vary with R (Franck-Condon approximation). In that case, the transition moment of Eq. (24) and therefore the cross section exactly reflect the bell-shaped behaviors of P_i and P_i^2, respectively. In the present paper, the Franck-Condon approximation will *not* be invoked, so that we shall present results that are exact or δ approximated with respect to the nuclear degree of freedom.

Until this point our description has referred uniquely to the molecular frame where the wave functions are more easily described. However, DPI is detected in the laboratory so that a transformation from the body-fixed to the space-fixed frames must be carried out. After this transformation, the previously defined vibronic states [Eqs. (1) and (4)] are seen as rovibronic states in the laboratory frame. As the recent experiments are not rotationally resolved, it is worthwhile to sum over the final rotational states and average over initial vibronic-state distribution. Assuming Hund's coupling case (b) and neglecting the vibration-rotation interaction, it can be demonstrated[16] that the above formulas are still valid in the laboratory frame.

By use of Eqs. (19) and (23), we obtain the cross section for the production of a final state defined by the collective symbol $\mathcal{F}$ defined in Eq. (18). In fact, the recent experiment of Dujardin *et al.*[17] does not resolve the final state so precisely. Hence, the partial cross section of Eq. (19) has to be summed and integrated over relevant degenerate final states. The discrete summations are over the selected configurations $\varepsilon l\,\varepsilon'(l+1)$, and over the three states ($^1\Sigma_u^+$, $^1\Pi_u^{\pm 1}$) comprised in each configuration.

The continuous summations are concerned with the energy variables and are slightly more involved. By impact with photons of energies E_γ, a final state of total energy E_f is reached. Within our model assumptions, the law of energy conservation reads

$$E_f = \varepsilon+\varepsilon'+E_f^n = E_\gamma + E_i \ . \tag{25}$$

A priori, any partitioning of E_f between the electronic and nuclear degrees of freedom is allowed. Taking into account of Eq. (25) in the integration over continuous energies, yields

$$\sigma^{2+}(E_\gamma) = \int_0^{E_f}\int_0^{E_f}\int_0^{E_f} \delta(\varepsilon+\varepsilon'+E_f^n-E_\gamma-E_i) \times d^3\sigma^{2+}(\mathcal{F},E_f^n \mid E_\gamma) \ . \tag{26}$$

The effect of the Dirac distribution is to select the energies ε, ε', and E_f^n, in accordance with Eq. (25). Consequently, the triple integral in Eq. (26) actually reduces to a double one. Alternate forms are possible for this integral, depending on the choice of the two independent variables among the set $\{\varepsilon,\varepsilon',E_f^n\}$. We have found it convenient to consider the energy ε of the electron with angular momentum l, and E_f^n, the nuclear energy, as the independent variables. Thus Eq. (26) can be rewritten as

$$\sigma^{2+}(E_\gamma)=\frac{4\pi^2\alpha a_0^2}{3}\sum_{l=0}^{\infty}\int_0^{E_f}d\varepsilon\int_0^{E_f-\varepsilon}dE_f^n\left[\sum_S\frac{\partial^2 f(S,l,\varepsilon,E_f-E_f^n-\varepsilon,E_f^n\mid E_\gamma)}{\partial\varepsilon\partial E_f^n}\right]. \tag{27}$$

Casting Eq. (27) into the form

$$\sigma^{2+}(E_\gamma)=\int_0^{E_f}\left\{\sum_{l=0}^{\infty}\frac{d\sigma^{2+}(l,\varepsilon\mid E_\gamma)}{d\varepsilon}\right\}d\varepsilon\ , \tag{28}$$

we retrieve, in a generalized form, the one-dimensional differential cross section $d\sigma^{2+}/d\varepsilon$ introduced in our preceding paper.

Now, permuting the order of integrations in Eq. (27), allows us to get information on the nuclear motion. This leads to

$$\sigma^{2+}(E_\gamma)=\frac{4\pi^2\alpha a_0^2}{3}\sum_{l=0}^{\infty}\int_0^{E_f}dE_f^n\int_0^{E_f-E_f^n}d\varepsilon\left[\sum_S\frac{\partial^2 f(S,l,\varepsilon,E_f-E_f^n-\varepsilon,E_f^n\mid E_\gamma)}{\partial\varepsilon\partial E_f^n}\right], \tag{29}$$

which is cast into a one-dimensional integral over the nuclear energy as

$$\sigma^{2+}(E_\gamma)=\int_0^{E_f}\left\{\frac{d\sigma^{2+}(E_f^n\mid E_\gamma)}{dE_f^n}\right\}dE_f^n\ . \tag{30}$$

In Eq. (30), $d\sigma^{2+}/dE_f^n$ provides us the distribution of kinetic energy of the nuclei, which is the major contribution of this paper with reference to paper I. It is worthwhile to emphasize that Eqs. (28) and (30) are perfectly symmetrical analyses of $\sigma^{2+}(E_\gamma)$, in spite of the very different physical natures of the electron- and proton-differential spectra, as will be seen in Sec. V. Of course, these analyses are also similar in form to the more familiar one involving the differential angular distribution $d\sigma^{2+}/d\Omega$.

Before ending this section, it is worthwhile to derive a simplified formula for the cross section at the onset. This is the first step towards the derivation of *molecular* threshold laws, analogous to the well-known Wannier-Rau-Peterkop (WRP) laws[18] for *atomic* processes. Our derivation rests upon two hypotheses related to the dynamics of electrons and nuclei, respectively. For the electrons, Roth[19] has applied the WRP laws to *atomic* multiple photoionization. He has found that the DPI cross section of a neutral atom varies above threshold as $\sigma^{2+}\propto(E_f^e)^{1.056}$, where E_f^e is the energy available for the outgoing electrons. As a first assumption, we suppose that such a dependence is also valid when electrons escape from the noncentral molecular field created by the two protons. As a consequence, the term $(E_f-E_f^n)^{1.056}$ can be factored out in the differential oscillator strength. The second hypothesis is that the δ approximation can be applied in the threshold region. Then, inserting both the matrix element obtained under the δ approximation [Eq. (24)], and the WRP dependence in the excess energy into Eq. (30), leads to

$$\sigma^{2+}(E_\gamma)=A\int_0^{E_f}\left\{\frac{P_i(v=0\mid 1/E_f^n)}{E_f^n}\right\}^2\times(E_f-E_f^n)^{1.056}dE_f^n\ , \tag{31}$$

where A is a constant factor. Equation (31) reveals that the total cross section for the DPI of a diatomic molecule varies at threshold as the convolution of the density probability in the initial vibrational ground state with a series of nearly linear electronic cross sections of the atomic type.

V. COMPUTATIONS

The practical application of the method described in the preceding sections involves a large amount of numerical calculation. All calculations have been done at the Computer Center (CIRCE) (Ref. 20) in Orsay.

The first computational step of the present work involves evaluation of accurately correlated electronic wave functions $\Phi_i(X\,^1\Sigma_g^+,R\mid \mathbf{r}_1,\mathbf{r}_2)$ [Eq. (1)] for the ground state of H_2. As in paper I, we used functions of the form optimized by Hagström and Shull,[10] i.e., 33-configuration mixings built up from 15 elliptic molecular orbitals. These electronic wave functions were computed for various internuclear separations by use of a configuration interaction program dealing with the nonorthogonal elliptical orbitals. The set of exponents optimized by Hagström and Shull for the equilibrium geometry ($R_e=1.4$ bohr) was used throughout. This set revealed to be of satisfactory accuracy since more than 95% of the correlation energy[9] is accounted for over internuclear separations ranging from 1.2 to 1.6 bohr. The energies so obtained are given in Table I, along with the corresponding SCF (Ref. 21) and exact theoretical values.[22]

The second computational step is the determination of the vibrational ground-state wave function $P_i(v=0\mid R)$. For this purpose, Eq. (2) was provided with the exact theoretical potential of Kolos and Wolniewicz,[22] and thence was solved by use of the Numerov-Cooley algorithm.[23] With an integration step length $\Delta R=0.01$ bohr and the integration range 0.4–4.0 bohr, we have obtained a vibrational energy $E_i^n(v=0)=0.009\,935$ hartree$\simeq$0.27 eV [Eq. (3)]. This yields a total ground-state energy of $-1.164\,539$ hartree, which compares well with the exact value $-1.164\,547$ hartree.[24] In Fig. 1, the potential for the $X\,^1\Sigma_g^+$ state of H_2 and the $v=0$ vibrational wave function are plotted as functions of the internuclear separation. The third numerical step is the computation of the final nuclear wave functions $P_f(E_f^n\mid R)$ for a set of

TABLE I. Potential energies and double-ionization potentials for various geometries of the $X\,^1\Sigma_g^+$ ground state of the hydrogen molecule. For the wave functions used in this work, the potential energies are followed by the percentage of correlation energy actually accounted for.

R (bohr)	Potential energies[a] (hartree) HF[c]	This work ($\%E_{corr}$)	Exact[a]	I^{2+}[b] (eV)
1.2	−1.125 029	−1.163 178(95.6)	−1.164 934	54.38
1.3	−1.132 024	−1.170 929(96.5)	−1.172 346	52.83
1.4	−1.133 630	−1.173 130(96.7)	−1.174 475	51.40
1.5	−1.131 375	−1.171 475(96.7)	−1.172 854	50.06
1.6	−1.126 352	−1.167 116(96.5)	−1.168 582	48.81

[a] $E_i^e(R)+1/R$, in the notation of the main text.
[b] $I^{2+}=-E_i^e$ for two-electron systems with fixed nuclei (see text).
[c] Hartree-Fock results from Ref. 21.
[d] Exact results from Ref. 22.

given positive energies $\{E_f^n\}$. As in the case of the bound vibrational state, these wave functions could have been obtained by the straightforward integration of Eq. (6). However, as mentioned in Sec. III, these functions are, in fact, well-known spherical Coulomb functions, within a normalizing factor. We took advantage of this in using an efficient specialized algorithm[25] for their computation. The repulsive potential of H_2^{2+} and its dissociation limit $H^+ + H^+$ are plotted in Fig. 1 with three continuum nuclear wave functions having the energies 0.4, 0.714, and 1.0 hartree (their corresponding classical turning points are 2.5, $R_e=1.4$, and 1.0 bohr, respectively).

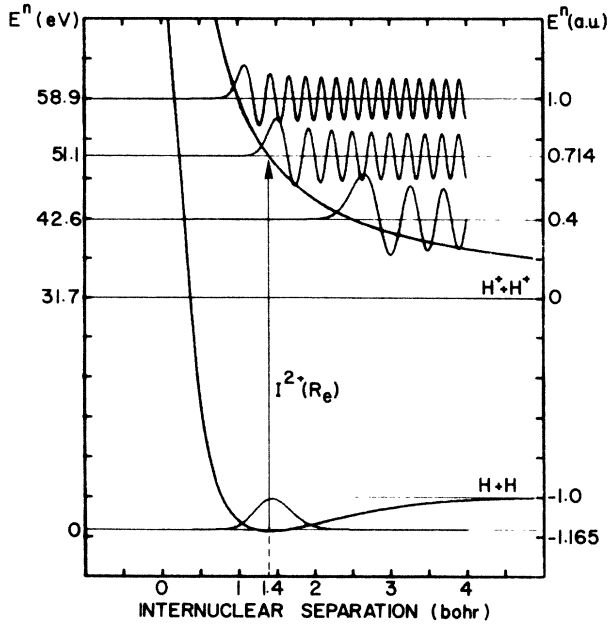

FIG. 1. Exact potential-energy curves for the neutral $H_2(^1\Sigma_g^+)$ and doubly ionized H_2^{2+} states of the molecular hydrogen (denoted by E_i^n and E_f^n, respectively, in the main text). Potentials are given in eV from the $v=0$ ground state of H_2 and in hartrees from the dissociation limit $H^+ + H^+$. The internuclear separation is in bohrs; the equilibrium value is $R_e=1.4$ bohr. The bound vibrational wave function $P_i(v=0)$ and three-continuum nuclear wave functions $P_f(E_f^n)$ are also plotted (on a different scale).

In order to check the vibrational part of our computational code, and also to verify numerically that the continuum nuclear wave functions given in Eqs. (10) and (11) are properly normalized, we found it convenient to use the closure property as a check. It was verified that a set of 18 energies ranging from 0.3 to 1.6 hartree correctly spans the relevant continuous spectrum. More precisely, we obtained the following numerical result:

$$\int_{0.3}^{1.6} |\langle P_f(E_f^n)(|P_i(v=0)\rangle|^2 dE_f^n \simeq 0.999\,92\ . \tag{32}$$

In computing the above integral, the values of the matrix elements were first calculated on the grid of the 18 selected energies, and the intermediate values were interpolated by cubic splines. For the actual calculation of cross sections, via the discretization of integrals over E_f^n, further tests have shown that a convenient set $\{E_f^n\}$ of proton energies consists in a grid of 51 equispaced values from 0.36 to 1.36 hartree (step length $\Delta E=0.02$ hartree). This choice ensures that the region where the initial vibrational state has significant amplitude (see Fig. 1) is spanned with sufficient accuracy.

At this stage, we have determined the final-state configurations $\varepsilon l\,\varepsilon'(l+1)$ that are significantly populated by the DPI process. Taking advantage of the fact that the DPI cross sections of helium and H_2, in the fixed equilibrium geometry, are rather similar (see paper I), the tests were made on the simpler helium case. A well-correlated initial ground-state wave function,[26] and three final channels $\varepsilon s\,\varepsilon' p$, $\varepsilon p\,\varepsilon' d$, and $\varepsilon d\,\varepsilon' f$ were used. At a photon energy of 100.8 eV, a total cross section of 0.553 10^{-2} Mb has been obtained, in accordance with the work of Byron and Joachain.[4] In this value, corresponding to the region where the cross section is maximum, the relative contributions of the final channels were found to be of 84.8% ($\varepsilon s\,\varepsilon' p$), 15.1% ($\varepsilon p\,\varepsilon' d$), and 0.14% ($\varepsilon d\,\varepsilon' f$). Hence, we decided to consider only the two first final configurations, which amount to summing over $l=0,1$ in Eqs. (27) and (29).

We now arrive at the major part of the numerical effort involved in the present study. The application of cross-

section formulas derived in Sec. IV requires several repeated integrals, since one has to sum over the electron coordinates, the internuclear distance, and two variables taken among the set $\{\varepsilon,\varepsilon',E_f^n\}$ depending on the way chosen for analyzing the total cross section [Eqs. (28) or (30)]. Fortunately, the computational effort implied in the evaluation of partial, differential, and total cross sections can be considerably reduced in the following way.

For the grid of internuclear distances given in Table I, the electronic dipole matrix elements $\underline{M}^e_{L,V}$ of Eqs. (23) or (24) are evaluated at fixed energies ε and ε', each of them ranging from 0.0 to 2.0 hartree with a step length of 0.1 hartree. The total dipole matrix elements $\underline{M}_{L,V}$ are then computed, via Eq. (22), for the previously determined grid of 51 final nuclear energies. All the required electronic matrix elements [Eqs. (23)] have been computed with an integral generator[27] previously used in the context of simple photoionization studies of H, H_2^+, and H_2.[28–30] It should be noted that the electronic dipole-matrix element $\underline{M}^e_{L,V}$ varies almost linearly with the internuclear separation. This allowed us to employ only the five geometries given in Table I. At this point, ignoring the various discrete indices that define the final states, one has obtained a three-dimensional matrix $\underline{M}^e_{L,V}(\varepsilon,\varepsilon',E_f^n)$ over $21\times21\times51$ preselected continuum energies. In order to make the last computational step more efficient, it is convenient to have the same step length $\Delta E=0.02$ hartree in the three dimensions. For this purpose, the matrix is enlarged by cubic-spline interpolation to a $101\times101\times51$ dimensional $\underline{M}^e_{L,V}$ matrix.

Until now, all computations have been done *without* any reference to the photon energy. The last numerical step consists in selecting all the matrix elements relevant to a given photon energy E_γ. This amounts to collecting all elements of the large $\underline{M}^e_{L,V}$ matrix that satisfy the law of conservation of energy [Eq. (25)]. These matrix elements are then conveniently summed in order to obtain the cross section, analyzed either in terms of electronic or nuclear energies [Eqs. (28) or (30), respectively].

VI. RESULTS AND DISCUSSION

The investigations reported in paper I have revealed that the dipole-length formulation is much less reliable than dipole-velocity one, as previously observed in the DPI of helium.[4] Consequently, we shall only report results obtained within the dipole-velocity formulation in the following. Some comparisons of the two forms are given in paper I. In this previous paper, the DPI of the H_2 molecule had been studied within a model where the motions of nuclei were completely ignored. More precisely, it was supposed that the nuclei remained held at the ground-state equilibrium distance R_e while both electrons were ejected. In the present work, the nuclei are allowed to move in the (bound) initial as well as in the (free) final nuclear states. This conceptually modifies the fixed-nuclei model used previously. In order to make the connection between the two approaches more transparent, it is worthwhile to discuss first the threshold energy where DPI begins to appear.

In the fixed-nuclei model, the protons keep their potential energy $1/R$ during the overall process. Neglecting the vibrational energy of the $v=0$ level, the combination of Eqs. (3), (5), and (25) leads to the relation

$$E_f^e=E_\gamma+E_i^e(R)=E_\gamma-I^{2+}(R)\ , \tag{33}$$

since for two-electron systems, the double-ionization potential I^{2+} appears to be the opposite of the electronic ground-state energy. Hence, if the nuclei are fixed at the distance R apart, the DPI cross sections will start at a photon energy equal to $I^{2+}(R)$. Some values of the double-ionization potential are given in Table I. For instance, one has $I^{2+}(R_e)=51.4$ eV at the equilibrium ground-state geometry $R_e=1.4$ bohr. If the vibrational energy of the $v=0$ level is taken into account, $I^{2+}(R_e)$ is slightly modified and the value 51.1 eV is obtained. On the contrary, when the nuclear motions are considered, the DPI process is theoretically allowed from photon energies of $-E_i\simeq31.7$ eV. These values are exemplified in Fig. 1.

In Fig. 2, a set of curves representing the total cross section at various fixed geometries is plotted. When R increases, these curves are shifted towards lower photon energies, in accordance with the fact that the double-ionization potential $I^{2+}(R)$ is a decreasing function of R in the neighborhood of the equilibrium value R_e (see Table I). In a sense, the cross sections derived at fixed internuclei separations are fictitious, but it has been observed in the context of *simple* photoionization that the cross sections calculated at $R=R_e$ are in good agreement with those resulting from the inclusion of nuclear vibration in the target and in the produced ion.[31] Figure 2 re-

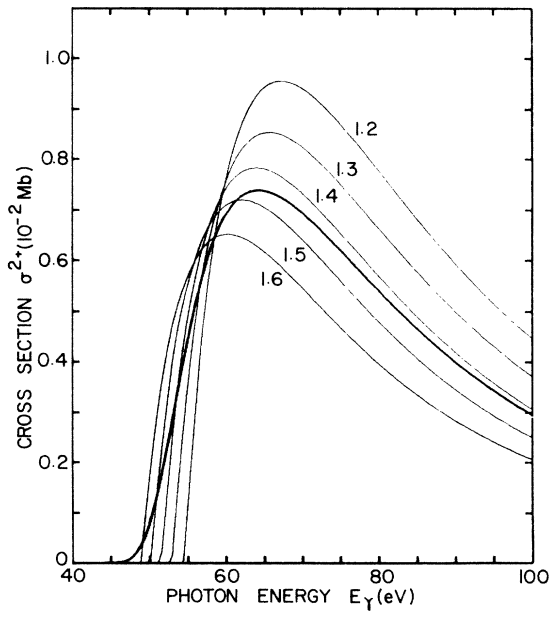

FIG. 2. Theoretical calculation of cross section σ^{2+} for molecular hydrogen in the velocity formulation. The solid curve corresponds to the calculation where the motion of nuclei is accounted for (R-averaged calculation). The dotted curves refer to calculations done within fixed geometries R between 1.2 and 1.6 bohr.

veals that this is also true for DPI. In this figure, the solid curve represents the actual theoretical cross section for which nuclear motion is properly taken into account. This curve has been obtained from Eqs. (28) and (30). We have verified numerically that both routes yield identical results. For brevity, this calculation will be denoted as the "R-averaged" result. As expected in paper I, the inclusion of initial nuclear vibration and final nuclear repulsion has a lowering effect on the cross section obtained at the fixed ground-state equilibrium geometry. However, this is a slight effect since the maximum in the total cross section decreases from 0.783 10^{-2} Mb to 0.739 10^{-2} Mb for photon energies of 64.0 and 64.3 eV, respectively. In contrast, the cross section increases in the region 45–50 eV which was energetically forbidden within the R_e-fixed calculation.

An enlargement of the threshold part of Fig. 2 is presented in Fig. 3. As expected in Sec. IV, it is found that the cross sections computed within *fixed* geometries are nearly linear functions of the excess energy, i.e., they obey the WRP atomic threshold law. The solid curve in Fig. 3 represents both the R-averaged and the δ-approximated curves since they actually differ by less than 1% over the whole energy range considered in this paper (40–100 eV). It can be seen that the slopes of these theoretical cross sections do no longer exibit a discontinuity, as was the case when nuclear motions were not accounted for. The dashed curve in Fig. 3 represents the molecular threshold law derived in Sec. V. The multiplicative constant A appearing in this law [Eq. (31)] has been determined by a matching with the exact cross section at 54 eV (this point is referred as P in Fig. 3).

From Fig. 4, it turns out that the molecular threshold law is of good accuracy over the photon energy range 45–55 eV. This is in accordance with the recent experiment of Lablanquie *et al.* on the DPI of argon,[32] whereas Roth[19] estimated that the range of validity of threshold law could be limited to 1.3 eV above threshold. Moreover, it should be noted that the extrapolation of the straight part of the R-averaged cross section does not yield the Franck-Condon value of the double-ionization potential $I^{2+}(R_e)=51.4$ eV, but a significantly lower value of 49.3 eV. As a consequence, caution must be exercised when extrapolating such linear parts of the cross section in predicting the existence of multiple electronic states of a doubly charged ion.[33]

In Fig. 5, we have plotted the total and partial cross sections obtained in the model of paper I for molecular hydrogen with the fixed equilibrium ground-state geometry $R=R_e$, for photon energies in the range 40–100 eV. As mentioned above, the total cross section has a maximum of 0.783 10^{-2} Mb for 64.0-eV photons. The relevant partial cross sections are associated with the $\varepsilon s\,\varepsilon' p$ and $\varepsilon p\,\varepsilon' d$ channels, as discussed in Sec. VI. It can be seen that the contribution of the $\varepsilon s\,\varepsilon' p$ states is greater by a factor of 3 near the maximum. However, as could be expected, the relative importance of the $\varepsilon p\,\varepsilon' d$ excitations becomes larger as the photon energy increases.

In Fig. 6, the R-averaged total cross section is compared with the very recent experimental results of Dujardin *et al.*[17] The agreement is rather good considering the approximations made in the present work, as well as the experimental uncertainties.

As explained in Sec. IV, the total cross section at a

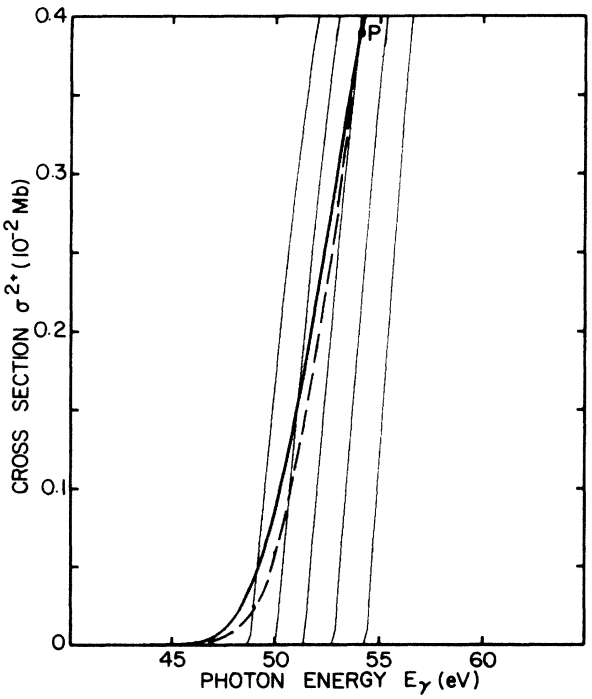

FIG. 3. Same as Fig. 2, but enlarged in the threshold region. The dashed curve corresponds to the molecular threshold law [Eq. (31)] matched onto the exact theoretical result at point P.

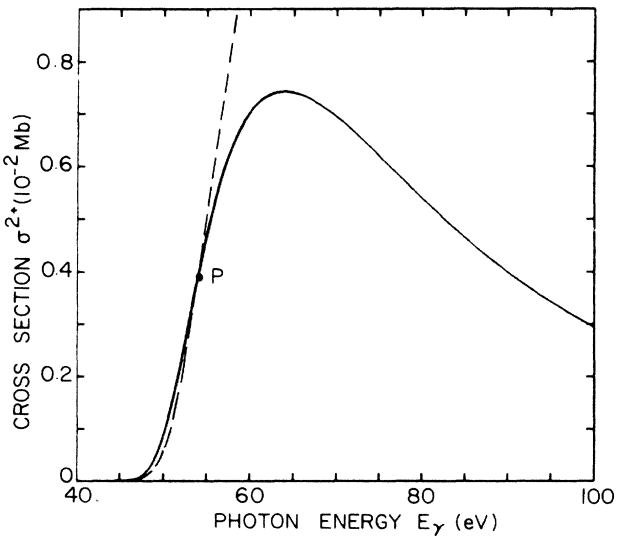

FIG. 4. Comparison of the cross sections σ^{2+} derived from the molecular threshold law (dashed curve) with the R-averaged one (solid curve) over the whole photon-energy range. Note that point P is the same as in Fig. 3, and that the δ-approximated curve is so close to the exact one that they cannot be distinguished in this figure.

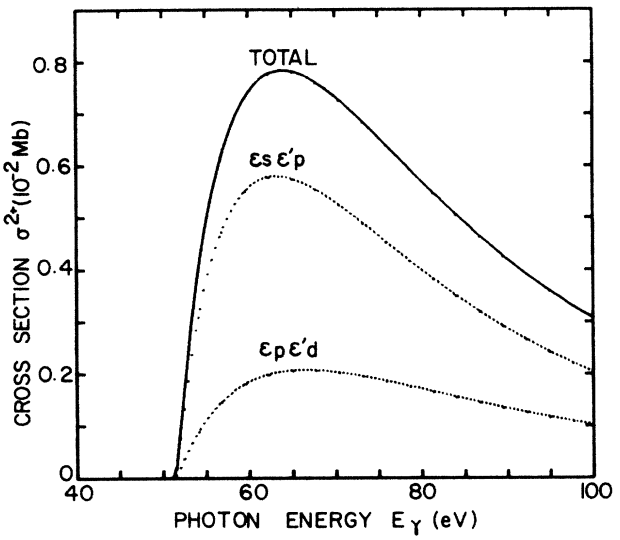

FIG. 5. Theoretical calculation of cross section σ^{2+} for molecular hydrogen in the fixed ground-state equilibrium geometry $R_e = 1.4$ bohr (velocity formulation). The dotted curves represent the contributions of the $\varepsilon s\ \varepsilon' p$ and $\varepsilon p\ \varepsilon' d$ pairs of ejected electrons. The solid curve is the total cross section (same as in Fig. 2).

given photon energy can be analyzed in terms of either photoelectron or proton kinetic energies. In paper I, due to the fixed-nuclei model, the latter analysis could not to be considered while the former was considerably simplified. Combining Eqs. (12) and (32) for $R = R_e$ leads to

$$\varepsilon + \varepsilon' = E_\gamma - I^{2+}(R_e) \ . \tag{34}$$

Equation (34) indicates that, in the model of paper I, given a photon energy of, say, $E_\gamma = 94.9$ eV, photoelectrons share the definite total kinetic energy $\varepsilon + \varepsilon' = 1.6$ hartree. The corresponding distribution of photoelectron energy had been calculated and is recalled in Fig. 7 (dotted curves). From this figure, it can be seen that the sharing of the total kinetic energy between the two ejected electrons is qualitatively different for the $\varepsilon s\ \varepsilon' p$ and $\varepsilon p\ \varepsilon' d$ pairs of ejected electrons. In the former case, the curve is highly peaked at its edges, indicating that an unequal sharing of energy is favored. One electron is likely to be ejected with most of the available energy ($\varepsilon \simeq 1.6$ hartree) while the other one barely escapes ($\varepsilon \simeq 0$). Furthermore, one observes that the curve of the channel $\varepsilon s\ \varepsilon' p$ is approximately symmetrical about the midpoint $\varepsilon = 0.8$ hartree. This demonstrates that events in which the slow electron is s and the more energetic one is p have almost the same probability of occurrence as those in which the slow electron is p and the energetic one is s. In contrast, for an $\varepsilon p\ \varepsilon' d$ pair of photoelectrons, the slow electron would necessarily be of the d symmetry since the differential oscillator strengths for a p electron with energies $\varepsilon = 1.6$ hartree and $\varepsilon = 0$ are almost in the ratio 17:1.

Let us now examine the photoelectron energy distribution derived within the present model which does account for the motions of nuclei. For a photon energy of 94.3 eV, very close to the preceding value, the differential cross sections $d\sigma^{2+}/d\varepsilon$ have been computed according to Eqs. (27) and (28) for the main two channels. The cor-

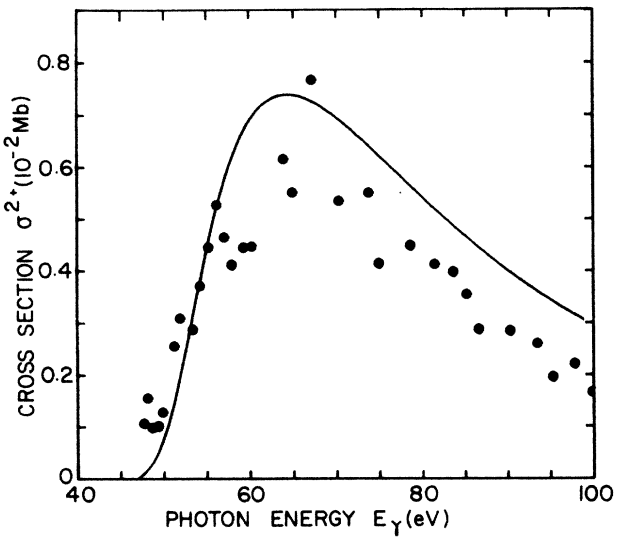

FIG. 6. Total cross section σ^{2+} for double photoionization of molecular hydrogen. The solid curve is the R-averaged calculation. Experimental data points are from Dujardin *et al.* (Ref. 17).

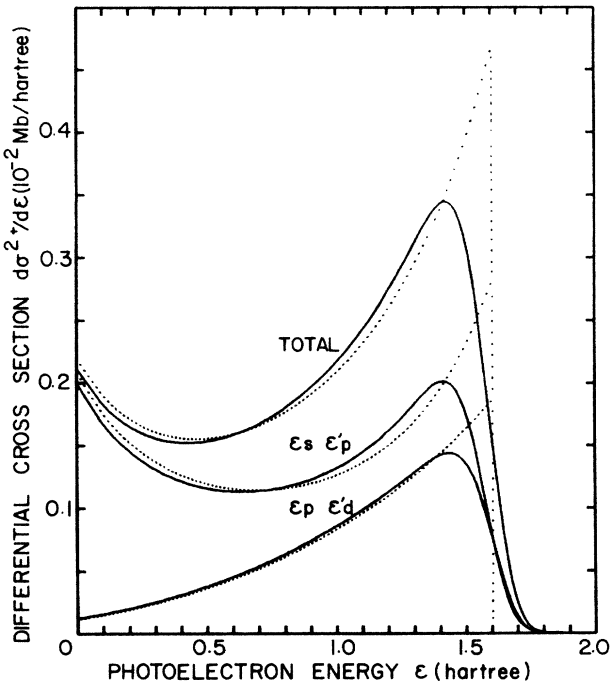

FIG. 7. Distribution of photoelectron kinetic energies calculated for 64.6-eV impacting photons. The partial contributions due to the $\varepsilon s\ \varepsilon' p$ and $\varepsilon p\ \varepsilon' d$ channels, as well as the total distribution are calculated within two different models: dotted curves refer to the vertical transition at the fixed ground-state equilibrium geometry R_e (from Ref. 3); solid curves are from the R-averaged calculation (this work).

responding curves are given in Fig. 7 (solid curves). From this figure, it is apparent that the conclusions drawn in paper I are confirmed by the more refined model used here. However, Fig. 7 reveals that curves are significantly cut down around their maxima at $\varepsilon \simeq 1.6$ hartree. This phenomenon is a consequence of the fact that the energy conservation law actually applies to the whole four-particle set $\{H^+ + H^+ + e^- + e^-\}$ instead of the two-electron set. Hence, the possibility now exists for the protons to have an energy less than the previous value $1/R_e$. Correspondingly, electrons can share this additional energy so that their kinetic energy can exceed 1.6 hartree.

It should be noted that electron kinetic energy distributions have not yet been measured for *molecular* DPI processes. In contrast, such experimental data are available for *atomic* DPI (Refs. 32 and 34) and, generally, compare well with the theoretical results obtained from many-body perturbation theory.[35]

We now turn to the analysis of the total cross section in terms of the two-proton kinetic energies. Equations (29) and (30) define the absolute differential cross section $d\sigma^{2+}/dE_f^n$ at a given photon energy. In Fig. 8, such curves are plotted for selected photon energies in the range 64.3–91.5 eV. From this figure, it can be seen that the favored two-proton kinetic energy is very slightly displaced towards higher energy for increasingly energetic photons. More precisely, it is found that the most probable two-proton energy increases regularly from 0.703 to 0.717 hartree over the considered photon energy range. This amounts to a displacement of 0.36 eV for the favored proton energy. As could be expected, the most probable value remains around $1/R_e \simeq 0.714$ hartree $\simeq 19.3$ eV. The shape of the curves of Fig. 8 and of the $v=0$ vibrational ground-state curve (Fig. 1) are clearly very similar. For instance, one recognizes in Fig. 8 the asymmetrical part of the vibrational function that reflects the anharmonicity of the exact potential. This strong analogy confirms that the δ approximation is valid in this actual problem. This is again confirmed in Fig. 9 where exact proton energy distributions are compared with the δ approximated ones. The upper curves are for 64.3 eV impacting photons, and so correspond to the maximum in the total section (see Fig. 2). In this energy region, the δ approximation provides an accurate reproduction of the proton kinetic-energy distribution since the relative error is less than 2%. For a photon energy of 53.5 eV, which corresponds to the threshold region, the lower curves show that the δ approximation is less satisfactory since the exact curve is now reproduced within a relative error of 7%. It should be noted that the latter curves are truncated above $E_f^n = 0.8$ hartree. This again relies on energy conservation. From Eq. (25) it is found that 53.5-eV photons populate final states with a total energy 0.8 hartree. This value is reached when both electrons are at rest, and is an upper bound for the two-proton energy.

Proton kinetic-energy distributions resulting from DPI of molecules have not yet been measured. However, such

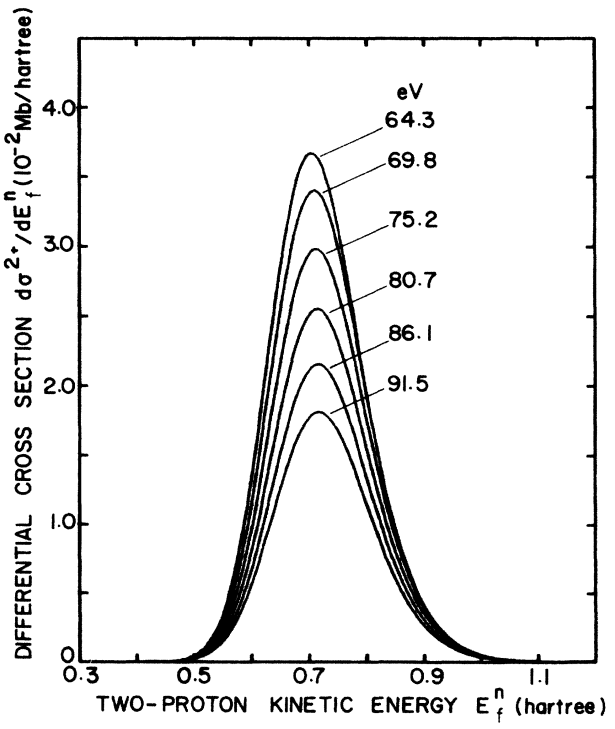

FIG. 8. Distributions of the two-proton kinetic energy E_f^n calculated for photon energies ranging from 64.3 to 91.5 eV.

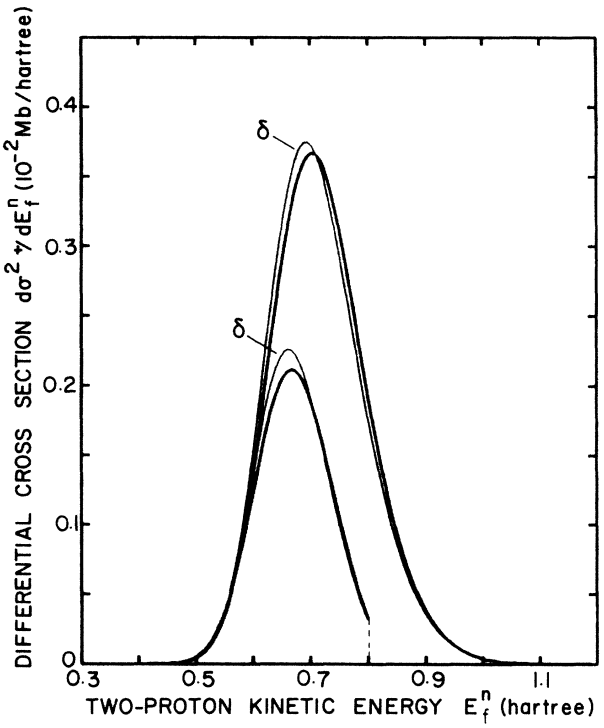

FIG. 9. Comparison of exact and δ approximated distributions of the two-proton kinetic energy E_f^n. The upper curves are for 64.3-eV photon energy, i.e., correspond to the region where the total cross section is maximum. The lower curves are for 53.5-eV photon energy, i.e., correspond to the threshold region. Note that 53.5-eV photons create final states with a total energy of 0.8 hartree. This value is then an upper bound for the two-proton energy range.

data are available (in arbitrary units) for the double ionization of the hydrogen molecule by electron[36] and proton[37] impact. In both experiments, it is found that (i) the proton kinetic-energy distributions have the expected bell shape and (ii) the abscissa of the maximum are not significantly modified when the energies of the projectiles are varied in the ranges 0.5–1 KeV and 3–9 KeV for the electron and proton, respectively. It should be noted that Fig. 8 revealed a quite similar behavior for impacting photons with a sufficiently high energy, say, larger than 60 eV. In contrast, Fig. 9 shows that the most probable two-proton kinetic energy is increased by 1.0 eV when going from 53.3 to 64.3 eV photons, i.e., when passing from the threshold region to the vicinity of the maximum in the total cross section.

VII. CONCLUSIONS

An *ab initio* calculation of the double photoionization of molecular hydrogen is presented. Partial and total cross sections are calculated in the 40–100 eV photon-energy range. Furthermore, at any given photon energy, the present model allows the total cross section to be analyzed in two complementary ways: (i) the photoelectron kinetic-energy distributions are obtained for the $\varepsilon s\,\varepsilon' p$ and the $\varepsilon p\,\varepsilon' d$ channels, (ii) the two-proton kinetic-energy distribution is extracted, either exactly or by use of the δ approximation, which is shown to be very accurate. In addition, the analytic expression of the *molecular* threshold law for DPI has been derived. In the case of H_2, this law is valid over a range of, say, $\simeq 10$ eV.

The theoretical cross section obtained here compares rather well with the absolute total cross section measured by Dujardin *et al.*[17] To date, this has been the sole available experimental observable concerning the DPI of the hydrogen molecule. As a consequence, our analyses of kinetic-energy distributions of fragments cannot be directly checked against experiment. However, the photoelectron energy distributions are very similar in shape to the *atomic* ones, except in the region of higher photoelectron energies where a purely *molecular* effect appears, namely, the possibility of a (small) exchange of energy between protons to electrons. On the other hand, the proton-energy distributions present a strong analogy with those resulting from electron and proton impact on H_2. Nevertheless, it is difficult to estimate the accuracy of the present model. Assuming that the Born-Oppenheimer separation is valid for dissociative DPI, it is likely that the major approximation made here lies in the *uncorrelated* electronic part of the final states. Hence, a relevant check of the method would result in the comparison of the present results with those deriving from the use of more refined wave functions for the double electronic continuum. A similar verification has been done for the DPI of helium,[38] since partly correlated two-free-electron wave functions are available in this case.[39] However, finding accurately correlated wave functions for atomic and molecular states with two-ejected electrons is a considerable challenge for theoricians. As a consequence, the many-body perturbation theory would be an attractive alternative to the wave-function approach for the *molecular* DPI, as it was proved to be the case for helium.[40]

ACKNOWLEDGMENTS

The author acknowledges G. Dujardin, Ch. Jungen, S. Leach, H. Lefebvre-Brion, I. Nenner, and G. Raseev for helpful comments on this manuscript.

APPENDIX

The purpose of this appendix is to normalize, in the energy scale, the approximate nuclear function $\delta(R-R_n)$ describing the repulsive two-proton state

$$P_f(E_n \mid R) \simeq \mathcal{N}(E_n)\delta(R-R_n) . \tag{A1}$$

Other derivations are available but they often use arguments like the vibration sum rule.[41] The present derivation is a purely mathematical one and is based only upon the basic properties of the Dirac distribution.

In Eq. (A1), E_n is the energy, in hartrees,[12] of the considered state and R_n the corresponding classical turning point ($R_n = 1/E_n$). The normalization factor is determined by the condition

$$\int_0^\infty P_f(E_n \mid R) P_f(\tilde{E}_n \mid R) dR = \delta(E_n - \tilde{E}_n) . \tag{A2}$$

Inserting the δ functions in the normalizing integral leads to

$$\int_0^\infty P_f(E_n \mid R) P_f(\tilde{E}_n \mid R) dR = \mathcal{N}(E_n)\mathcal{N}(\tilde{E}_n)\delta(R_n - \tilde{R}_n) . \tag{A3}$$

by use of a fundamental property of the Dirac distribution.[42] Moreover, using

$$\delta\left[\frac{1}{x} - a\right] = \frac{1}{a^2}\delta\left[x - \frac{1}{a}\right] , \tag{A4}$$

which is a particular case of the theorem giving $\delta[f(x)]$,[42] we get

$$\delta(R_n - \tilde{R}_n) = \delta\left[\frac{1}{E_n} - \tilde{R}_n\right] = \frac{1}{\tilde{R}_n^2}\delta\left[E_n - \frac{1}{\tilde{R}_n}\right] = \tilde{E}_n^2 \delta(E_n - \tilde{E}_n) . \tag{A5}$$

Finally, the right-hand side of Eq. (A3) becomes

$$\mathcal{N}(E_n)\mathcal{N}(\tilde{E}_n)\tilde{E}_n^2 \delta(E_n - \tilde{E}_n) = \mathcal{N}(E_n)^2 E_n^2 \delta(E_n - \tilde{E}_n) , \tag{A6}$$

by use of the property $f(x)\delta(x-a) = f(a)\delta(x-a)$. In order to arrive at the correct normalization $\delta(E_n - \tilde{E}_n)$, we are led to

$$\mathcal{N}(E_n) = \frac{1}{E_n} , \tag{A7}$$

which is the result used in the main text.

[1]G. Dujardin, S. Leach, O. Dutuit, P. M. Guyon, and M. Richard-Viard, Chem. Phys. **88**, 339 (1984); P. Lablanquie, I. Nenner, P. Millie, P. Morin, J. H. D. Eland, M. J. Hubin-Franskin, and J. Delwiche, J. Chem. Phys. **82**, 2951 (1985); G. Dujardin and D. Winkoun, *ibid.* **83**, 6222 (1985); G. Dujardin, D. Winkoun, and S. Leach, Phys. Rev. A **31**, 3027 (1985); D. Winkoun and G. Dujardin, Z. Phys. D **4**, 57 (1986); P. Millie, I. Nenner, P. Archirel, P. Lablanquie, P. Fournier, and J. H. D. Eland, J. Chem. Phys. **84**, 1259 (1986); P. J. Richardson, J. H. D. Eland, P. G. Fournier, and D. L. Cooper, *ibid.* **84**, 3189 (1986); G. Dujardin, L. Hellner, D. Winkoun, and M. J. Besnard, Chem. Phys. **105**, 291 (1986).

[2]See most of the papers of quoted in Ref. 1, and, e.g., P. W. Thulstrup, W. E. Thulstrup, A. Andersen, and Y. Öhrn, J. Chem. Phys. **60**, 3975 (1974); N. H. F. Beebe, E. W. Thulstrup, A. Andersen, and Öhrn, *ibid.* **64**, 2080 (1976); R. W. Wetmore, R. J. Le Roy, and R. K. Boyd, *ibid.* **88**, 6318 (1984); R. W. Wetmore, R. K. Boyd, and J. Le Roy, Chem. Phys. **89**, 329 (1984); R. W. Wetmore and R. K. Boyd, J. Chem. Phys. **90**, 5540 (1986); **90**, 6091 (1986); D. L. Cooper, Chem. Phys. Lett. **132**, 377 (1986).

[3]H. Le Rouzo, J. Phys. B **19**, L677 (1986).

[4]F. W. Byron and C. J. Joachain, Phys. Rev. **164**, 1 (1967).

[5]As a general rule, in a symbol like $(a \mid b)$, b will refer to an actual set of variables while a will stand for a set of actual parameters or indexes. As an example, R is a variable in vibrational functions $P(\cdots \mid R)$ but becomes a parameter in the electronic ones $\Phi(R \mid \cdots)$.

[6]Atomic units for length and energy are 1 bohr = 0.529 177 Å and 1 hartree = 27.211 65 eV, respectively. See B. N. Taylor, W. H. Parker, and D. N. Langenberg, Rev. Mod. Phys. **41**, 477 (1969).

[7]The correlation energy (E_{corr}) is usually defined as the difference $E_{\text{SCF}} - E_{\text{exact}}$, where E_{SCF} is the (closed-shell) Hartree-Fock energy and E_{exact} the exact (nonrelativistic) energy.

[8]R. L. Brown, Phys. Rev. A **1**, 586 (1970).

[9](a) For He ($1\,^1S_0$) one has $E_{\text{SCF}} = -2.861\,68$ hartree [C. J. Roothaan and A. W. Weiss, Rev. Mod. Phys. **32**, 194 (1960)] and $E_{\text{exact}} = -2.903\,72$ hartree [T. Kinoshita, Phys. Rev. **105**, 1490 (1957)], hence, $E_{\text{corr}} = 0.042\,04$ hartree. (b) For $H_2(X\,^1\Sigma_g^+ \mid R_e)$ one has $E_{\text{SCF}} = -1.133\,57$ hartree [W. Kolos and C. J. Roothaan, Rev. Mod. Phys. **32**, 205 (1960)] and $E_{\text{exact}} = -1.174\,47$ hartree [W. Kolos and L. Wolniewicz, J. Chem. Phys. **49**, 404 (1968)], hence, $E_{\text{corr}} = 0.040\,90$ hartree at the equilibrium geometry $R_e = 1.4$ bohr.

[10]S. Hagström and H. Shull, Rev. Mod. Phys. **35**, 624 (1963).

[11]*Handbook of Mathematical Functions* edited by M. Abramowitz and I. A. Stegun, (Dover, New York, 1965).

[12]The fact that energies are expressed in hartrees (See Ref. 6) is accounted for in the Dirac normalization. If rydberg units are used (1 hartree = 2 Ry), the normalizing factors of wave functions must be divided by $\sqrt{2}$.

[13]E. U. Condon, Phys. Rev. **32**, 858 (1928). The δ or reflection approximation has been applied to dissociative ionization of diatomic molecules by H. D. Hagstrum and J. T. Tate, Phys. Rev. **59**, 354 (1941).

[14]A. L. Ford, K. K. Docken, and A. Dalgarno, Astrophys. J. **195**, 819 (1975).

[15]A. C. Allison and A. Dalgarno, J. Chem. Phys. **55**, 4342 (1971).

[16]S. V. ONeil and W. P. Reinhardt, J. Chem. Phys. **69**, 2126 (1978).

[17]G. Dujardin, M. J. Besnard, L. Hellner, and Y. Malinovich, Phys. Rev. A **35**, 5012 (1987).

[18]G. H. Wannier, Phys. Rev. **90**, 817 (1953); A. R. P. Rau, Phys. Rev. A **4**, 207 (1971); R. Peterkop, J. Phys. B **4**, 513 (1971). A comprehensive review of the Wannier-Rau-Peterkop theory, by F. H. Read, can be found in *Electron Impact Ionisation*, edited by T. D. Märk and G. H. Dunn (Springer-Verlag, Berlin, 1985).

[19]T. A. Roth, Phys. Rev. A **5**, 476 (1972). In this paper, we are only concerned with $^1P^{\text{odd}}$ two-electron states. It should be noted that $^1P^{\text{even}}$ states have a different threshold behavior [see, e.g., C. H. Greene and A. R. P. Rau, J. Phys. B **16**, 99 (1983)].

[20]Centre Inter-Régional de Calcul Electronique du C. N. R. S., Boîte Postale **63**, 91406 Orsay Cédex, France.

[21]W. Kolos and C. C. J. Roothaan, Rev. Mod. Phys. **32**, 219 (1960).

[22]W. Kolos and L. Wolniewicz, J. Chem. Phys. **49**, 404 (1968).

[23]J. W. Cooley, Math. Computation **15**, 363 (1961).

[24]W. Kolos and L. Wolniewicz, J. Chem. Phys. **41**, 3674 (1964).

[25]A. R. Barnett, D. H. Feng, J. W. Steed, and L. J. B. Goldfarb, Comput. Phys. Commun. **8**, 377 (1974).

[26]R. K. Nesbet and R. E. Watson, Phys. Rev. **110**, 1073 (1958). This He($1\,^1S_0$) ground-state wave function gives an energy of $-2.902\,76$ and accounts for 97.7% of the correlation energy [see Refs. 7 and 9(a)].

[27]H. Le Rouzo (unpublished).

[28]H. Le Rouzo and G. Raseev, Phys. Rev. A **29**, 1214 (1984).

[29]H. Le Rouzo, Phys. Rev. A **32**, 650 (1985).

[30]G. Raseev, J. Phys. B **18**, 423 (1985).

[31]G. Raseev, H. Le Rouzo, and H. Lefebvre-Brion, J. Chem. Phys. **72**, 5701 (1980).

[32]P. Lablanquie, J. H. D. Eland, I. Nenner, P. Morin, J. Delwiche, and M. J. Hubin-Franskin, Phys. Rev. Lett. **58**, 992 (1987).

[33]M. J. Besnard, L. Hellner, Y. Malinovich, and G. Dujardin, J. Chem. Phys. **85**, 1316 (1986).

[34]T. A. Carlson, Phys. Rev. **156**, 142 (1967).

[35]T. N. Chang, T. Ishihara, and R. T. Poe, Phys. Rev. Lett. **27**, 838 (1971); T. N. Chang and R. T. Poe, Phys. Rev. A **12**, 1432 (1975); S. L. Carter and H. P. Kelly, *ibid.* **16**, 1525 (1977).

[36]K. E. McCulloh and H. M. Rosenstock, J. Chem. Phys. **48**, 2084 (1968); K. E. McCulloh, *ibid.* **48**, 2090 (1968).

[37]P. G. Fournier, H. Aouchiche, V. Lorent, and J. Baudon, Phys. Rev. A **34**, 3743 (1986).

[38]S. N. Tiwary, J. Phys. B **15**, L323 (1982).

[39]P. L. Altick, Phys. Rev. A **21**, 1381 (1980); **25**, 128 (1982); J. Phys. B **16**, 3543 (1983).

[40]S. L. Carter and H. P. Kelly, Phys. Rev. A **24**, 170 (1981).

[41]G. H. Dunn, Phys. Rev. **172**, 1 (1968).

[42]A. Messiah, *Quantum Mechanics* (North-Holland, Amsterdam, 1961), Vol. I. Appendix A.